Reduction in CD11c$^+$ microglia promotes clinical progression in autoimmune demyelination

Florian Mayrhofer[b], Zhanna Dariychuk[b], Anthony Zhen[b], Daniel J. Daugherty[a,b], Peter Bannerman[b], Angela M. Hanson[b], David Pleasure[b], Athena Soulika[b], Wenbin Deng[a,b], Olga V. Chechneva[a,b*]

[a]Department of Biochemistry and Molecular Medicine, UC Davis, Sacramento, CA 95817; [b]IPRM, Shriners Hospital for Children, Sacramento, CA 95817

Corresponding author:

Olga V. Chechneva

Department of Biochemistry and Molecular Medicine

School of Medicine, UC Davis

2425 Stockton Blvd, Sacramento, CA, 96817

Phone: 916-453-2250

Fax: 916-453-2288

Email: ochechneva@ucdavis.edu

Abstract

Multiple sclerosis (MS) is a chronic autoimmune demyelinating disorder. Most people with MS show a relapsing-remitting disease course that over time transitions into progressive decline of neurologic function. The mechanisms underlying disease progression in MS remain poorly understood. Here we demonstrate that reduction in CD11c$^+$ microglia promotes dispersed coalescent parenchymal infiltration and clinical progression in chronic mild experimental autoimmune encephalomyelitis (EAE), an animal model of MS. We found sex-dependent differences in EAE progression mediated by p38α signaling, a key regulator of inflammation. CD11c promoter-driven knockout of *p38α* (*KO*) reduced CD11c$^+$ microglia proliferation in female mice and promoted CNS infiltration and transition of chronic mild to severe disease. In protected *KO* males, immune cells were trapped within perivascular spaces and prevented from crossing the glia limitans closely surrounded by dendritic cell-like CD11c$^+$ microglia. Together, our study provides the first evidence that in chronic mild EAE, CD11c$^+$ microglia interact with astrocytes to control CNS immune cell parenchymal infiltration.

Keywords:
CD11c$^+$ microglia, chronic EAE progression, CNS infiltration, p38α sexual dimorphism, glia limitans

Introduction

Multiple sclerosis (MS) is an autoimmune demyelinating disorder characterized by chronic inflammation, myelin loss and axonal degeneration. MS is a complex pathological condition, with a high variability of clinical symptoms. In 80% of patients, MS appears as a relapsing-remitting form (RRMS) where episodes of neurologic dysfunction are separated by periods of remission (Baecher-Allan *et al.*, 2018). Within a decade of first diagnosis, the majority of RRMS patients develop progression of clinical deficits (Coret *et al.*, 2018; Zhang *et al.*, 2015). The pathologic mechanisms and specific cell types that are involved in the transition to progression are poorly understood (Trapp *et al.*, 1999).

$CD11c^+$ cells play an active role in the pathogenesis of MS. $CD11c^+$ classical dendritic cells (cDC) are professional antigen-presenting cells that present antigen and induce proliferation and polarization of naïve and effector T cells (Giles *et al.*, 2018a; Mundt *et al.*, 2019). Meningeal and perivascular cDC are responsible for the reactivation of myelin-primed T cells that drive clinical progression in experimental autoimmune encephalomyelitis (EAE), an animal model of MS (Giles *et al.*, 2018a; Greter *et al.*, 2005; Mundt *et al.*, 2019). Another subset, $CD11c^+$ monocyte-derived myeloid DC (moDC) emerge from $CD11b^+$ monocytes that infiltrate the CNS at EAE onset. moDC induce demyelination by producing iNOS-generated reactive oxygen species (Giles *et al.*, 2018b; King *et al.*, 2009). Before EAE remission, the majority of moDC undergo transcriptional reprograming toward an Arginase-1 expressing neuroprotective phenotype (Giles *et al.*, 2018b). moDC exert efficient phagocytic activity (Giles *et al.*, 2018a; Giles *et al.*, 2018b).

$CD11c^+$ microglia are resident in the healthy CNS and found in close proximity to astrocyte endfeet (Kamphuis *et al.*, 2016; Prodinger *et al.*, 2011; Wlodarczyk *et al.*, 2015). $CD11c^+$ microglia have poor antigen presenting capacity (Ford *et al.*, 1995; Giles *et al.*, 2018a; Greter *et al.*, 2005; Miller *et al.*, 2007). Increase in $CD11c^+$ microglia precedes the onset of EAE clinical symptoms (Fischer and

Reichmann, 2001; Serafini *et al.*, 2000). A growing number of evidences suggests that CD11c$^+$ microglia possess a neuroprotective function in disease. Increase in CD11c$^+$ microglia was associated with a reduction of EAE clinical disability (Wlodarczyk *et al.*, 2018), alleviation of cuprizone-induced demyelination (Sato-Hashimoto *et al.*, 2019), and cognitive improvement in a transgenic model of Alzheimer's disease (Butovsky *et al.*, 2006). The role of CD11c$^+$ microglia in MS progression remains unknown.

Among the key regulators of inflammation is mitogen-activated protein kinase 14 (p38α), a member of the p38 MAPK family (Zarubin and Han, 2005). Expression of p38α is upregulated in active and chronic lesions in patients with MS (Lock *et al.*, 2002). cDC depend on p38α signaling to promote differentiation of uncommitted T cells toward T_H17 phenotype in MS and EAE (Di Mitri *et al.*, 2015; Huang *et al.*, 2012) resulting in mild EAE phenotype in mice with knockout of *p38α* in CD11c$^+$ cells (Huang *et al.*, 2012; Krementsov *et al.*, 2014). A sex-dependent role of p38α in EAE has been reported in myeloid cells, where pharmacological inhibition or myeloid cell knockout of *p38α* ameliorated EAE clinical symptoms and inflammation in female mice (Krementsov *et al.*, 2014). A role of p38α signaling in CD11c$^+$ microglia has not been described.

Here we demonstrate that reduction in CD11c$^+$ microglia promotes the transition from chronic mild EAE to clinical progression with dispersed coalescent parenchymal infiltration. We identified a novel sex-dependent role of p38α in CD11c$^+$ microglia, where knockout of *p38α* resulted in a reduction in CD11c$^+$ microglia and promoted EAE progression in female mice. Our data further indicate that dendritic cell (DC)-like CD11c$^+$ microglia interact with astrocytes at the glia limitans to control immune cells infiltration into the CNS parenchyma in chronic autoimmune demyelination.

Materials and Methods

Animals

Female and male C57BL/6 mice 12 weeks old were used to study EAE progression in wild type (WT) mice. Mice carrying the *p38α floxed* allele ([B6.129-*Mapk14*<tm1.2Otsu], Riken #RBRC02192) were crossed with mice expressing Cre recombinase under the CD11c promoter ([C57BL/6J-Tg(*Itgax*-cre-EGFP)4097Ach/J], JAX stock #007567). Offsprings were genotyped for the presence of *p38α floxed* allele and *Cre* insert as described earlier (Lo *et al.*, 2014). Female and male $p38\alpha^{\Delta CD11c}$ (*KO*) and $p38\alpha^{fl/fl}$ (*floxed*) mice were used for experiments. Animals were maintained in accordance to the NIH Guide for the Care and Use of Laboratory Animals. Experimental protocols were approved by the Institutional Animal Care and Use Committee at the University of California, Davis.

EAE induction

EAE was induced in female and male mice at the age of 12 weeks as described earlier with some modifications (Chechneva *et al.*, 2011). In brief, mice were injected subcutaneously at two flank sites with an emulsion of MOG_{35-55} (New England Peptide) in incomplete Freund's adjuvant supplemented with 500 µg Mycobacterium tuberculosis H37Ra (Difco). MOG_{35-55} (300 µg) emulsion was prepared by quick sonication (3x5 sec on ice) or syringe emulsification. For syringe emulsification, MOG_{35-55} (150 µg) was homogenized in 2 syringes connected by a stopcock (twice 10 min with 3 h interval on ice). Emulsion was kept in the dark at 4^0C between mixing and before preparing into individual doses in syringes. Mice received 200 ng of pertussis toxin (PTX) (List Biological Labs) intraperitoneally (i. p.) on day 0 and 2. The severity of clinical symptoms was evaluated using following neurologic scoring system for EAE: 0 - no deficit; 0.5 - mild loss of tail tone; 1 - complete loss of tail tone; 1.5 - mildly impaired righting reflex; 2 - abnormal gait (ataxia) and/or impaired righting reflex; 2.5- single hind limb paresis and ataxia; 3 - double hind limb paresis; 3.5 - single limb paralysis and paresis of second limb / paresis of both hind limbs and weakness of front limbs;

4 - full paralysis of two limbs; 4.5 - hind limb paralysis with hind body paresis; 5 – moribund or death. Animals were monitored and scored daily.

Histology and pathological scoring

Histological analysis was performed as described earlier (Chechneva *et al.*, 2011). Briefly, mice were anesthetized with isoflurane and perfused with ice cold phosphate buffered saline (PBS). Lumbar spinal cords were dissected, cryopreserved in 20% sucrose, embedded in OCT compound and cut in 15 µm sections on the cryostat. For Luxol Fast Blue (LFB) staining, sections were incubated with 0.1% LFB solution at 60^0C for 16 h followed by differentiation with 0.05% lithium carbonate and co-stained with 0.1% Cresyl Violet. For Hematoxylin & Eosin (H&E) staining, sections were stained with Mayer's hematoxylin followed by 1% eosin. Slides were mounted using Cytoseal-60 medium and images were acquired on Keyence BZ-9000 microscope. For pathological assessment, for each animal, six sections of the lumbar spinal cord in the interval of 180 µm were scored by blinded investigator for infiltration, vacuolation caused by swollen axon sheaths and demyelination. We used following scoring system: 0 - absence of lesion and infiltration; 1 - not clearly visible lesions and infiltration, 2 – clearly visible lesions and infiltration, 3 – prominent multifocal lesions and infiltration, 4 – marked continuous lesions and infiltration (Shi *et al.*, 2011).

Immunohistochemistry

For immunostaining, sections were washed with PBS to remove residues of OCT compound. Nonspecific binding of antibodies was blocked using 10% normal serum in 0.2% Triton-X in PBS. Samples were incubated with rabbit anti-Iba1 (ionized calcium binding adaptor molecule 1; 1:500; Wako 019-19741), rabbit anti-CD4 (1:200; Abcam ab183685), rat anti-CD45 (1:200; SouthernBiotec 1660-01), FITC conjugated lectin from Lens culinaris (1:300; Sigma), chicken anti-GFP (1:500, Abcam ab13970), rat anti-CD11b (1:100, BD Pharmingen 550282), rabbit anti-CCL2 (1:200, Millipore AB1834P) overnight at 4 °C. Fluorophore-conjugated secondary antibodies Alexa Fluor

488, 555 or 647 (1:1000; Life Technologies) were used to detect primary antibody. Slides were mounted using DAPI Fluoromount-G (SouthernBiotech). Images were acquired on Nikon Eclipse TE 2000-E microscope using a D-Eclipse C1si camera (Nikon). For DAB staining, sections were treated with 1% H_2O_2 to stop endogenous peroxidase activity before incubation with blocking serum. After primary antibodies, sections were incubated with HRP-conjugated secondary antibody. Positive signal was visualized using ImmPACT DAB Peroxidase substrate kit (Vector labs). Images were acquired on Olympus BX61-DSU microscope using Hamamatsu ORCA-ER camera (Hamamatsu Photonics). For fluorescent and DAB staining negative controls omitting primary antibody were performed. Images were processed using Adobe Photoshop CC.

FACS analysis

Mice were deeply anesthetized and transcardially perfused with ice-cold PBS for 3 min with a flow rate at 3 ml/min. Brain and spinal cord were dissected and placed in ice-cold HBSS (Hank's Balanced Salt Solution) in 2.5 cm culture dish. For tissue digestion, papain resulted in a higher cell yield compared to collagenase. However, we found that papain digestion resulted in the loss of CD11c expression on the cell surface. Therefore, CNS tissue for all FACS experiments were digested using collagenase. Collagenase D (Roche) 1 mg/ml and 0.02 mg/ml with 100 U/ml DNAse I (Worthington) were added to each dish (final concentration), tissue was chopped into ~1-2 mm^3 pieces and incubated while shaking at 100 rpm at 37 °C with 5% CO_2 for 20 min. Enzymatic activity was blocked by EDTA at final concentration 2 mM. Tissue was homogenized in Dounce homogenizer (5-8 strokes) on ice and cell suspension was passed through a 100 µm cell strainer (Corning) in 50 ml falcon tubes. Cells were collected at 350 x g for 5 min at 4°C. To remove myelin and dead cells, cell pellet was resuspended in 37% Percoll (GE Healthcare). Cells were transferred to 15 ml falcon tubes and centrifuged at 500 x g for 15 min with 0 brake at 4^0C. Myelin layer was aspirated and cell pellet was resuspended in cold 0.5 ml RBC lysis buffer (Biolegend, 420301), transferred and incubated in 15

ml falcon tubes for 30 sec on ice. 5 ml PBS was added to each tube after incubation and cells were separated by centrifugation at 350 x g at 4^0C for 5 min. Cells were resuspended in FACS buffer (PBS plus 1% BSA and 0.1% sodium azide), counted using hemocytometer and transferred to staining plates (Fisher Scientific, 12565502). After 15 min blocking of Fc receptors with CD16/CD32 antibody (BD Pharmingen) on ice, cells were stained with fluorophore-conjugated antibodies: CD11b BV605 (1:200, clone M1/70, Biolegend), CD45 PerCP-Cy5.5 (1:200, clone 30-F11, Biolegend), Ly6G APC-Cy7 (1:200, clone 1A8, BD Biosciences), CD11c FITC (1:100, clone N418, Biolegend), CD11c APC (1:100, clone N418, Biolegend) on ice for 30-60 min. Cells were washed twice with FACS buffer and once with PBS to remove residues of BSA, then incubated with dead cell dye, Zombie red (1:1000 in PBS, Biolegend) for 15 min on ice. After washing, cells were analyzed on Attune NxT Acoustic Focusing Cytometer (Life Technologies). For cytokine detection, cells were counted and incubated in RPMI-1640 medium supplemented with 10% FBS, 2 mM glutamax, 1 mM sodium pyruvate, 0.1 mM NEAA, 100 U penicillin/streptomycin, 50 μM β-ME with Golgi plug (BD Biosciences, 555029) for 1 h at 37^0C with 5% CO_2. Phorbol 12-myristate 13-acetate (PMA, 50 ng/ml final concentration) and ionomycin (750 ng/ml final concentration) were added to incubate for 4-5 h at 37^0C. Fc receptors were blocked as described above and cells were stained with CD3e FITC (1:200, clone 145-2C11, BD Pharmingen) or CD3e PE-Cy7 (1:200, clone 145-2C11, BD Pharmingen). Dead cells were labeled using Violet fluorescence reactive dye for 20 min on ice (1:1000, ThermoFisher, Cat# L34963). Cells were fixed for 15 min on ice using BD Cytofix/Cytoperm reagent (BD Biosciences, 554722). After washing with BD Perm/Wash (BD Biosciences, 554723) twice, cells were incubated overnight at 4^0C with IFN-γ APC (1:25, Clone XMG1.2, Biolegends) and IL-17 PE (1:50, Clone TC11-18H10, BD Pharmingen) in Perm/Wash buffer. After washing with FACS buffer, cells were analyzed on Attune NxT Acoustic Focusing Cytometer (Life Technologies). Unstained cells, single stain controls and stained AbC Total Antibody Compensation beads (Thermo Fisher, A10497) were used for each experiment to determine compensation parameters. For isotype control

of fluorescence minus one, the specific antibody was substituted by fluorophore-conjugated isotype control. Acquired data were analyzed using FlowJo software (TreeStar). To define the population of $CD11c^+$ microglia, we found gating on $CD11b^+$ and $CD45^+$ cells from the pool of $CD11c^+$ cells was more accurate than gating of $CD11c^+$ cells from $CD11b^+CD45^{low}$ due to the lack of clear separation of macrophages/monocytes from microglia within $CD11b^+CD45^{int}$ population. The absolute number of specific cell types isolated from the CNS was determined by multiplying the total number of live cells to the proportion of the specific cell type acquired by flow cytometer. The quantitative data were presented in absolute numbers.

Proliferation assay of $CD11c^+$ cells

EdU is a thymidine nucleoside analog that incorporates into DNA during S-phase of the cell cycle. To label proliferating cells, animals were pulsed twice with 12 mg/kg EdU intraperitoneal injection in 12 h interval. 24 h after the first injection, animals were deeply anesthetized and perfused with ice cold PBS. Brain and spinal cord were dissected, and cells were isolated as described above. Fc receptors were blocked with CD16/CD32 antibody (BD Pharmingen) for 15 min on ice and cells were stained with fluorophore-conjugated antibodies: CD11b BV605 (1:200, clone M1/70, Biolegend), CD45 PerCP-Cy5.5 (1:200, clone 30-F11, Biolegend) and CD11c APC (1:100, clone N418, Biolegend) for 30 min on ice. Zombie violet (1:1000, Biolegend) was used to label dead cells. Cells were then fixed with 4% PFA for 15 min at RT. After washing with 1% BSA in PBS, cells were permeabilized with saponin-based permeabilization and wash reagent (Invitrogen, Click-iT Plus EdU Kit) for 15 min at RT. Residues of permeabilization buffer were removed by centrifugation at 350 x g for 5 min. EdU was detected by incubation with freshly prepared Click-iT cocktail containing Tris-HCl (100 mM, pH 7.6), 2 mM $CuSO_4$, 2.5 µM Sulfo-Cy3 Azide (Limiprobe) and 100 mM ascorbic acid for 15 min at RT in the dark. Cells were washed with FACS buffer and analyzed on Attune NxT Acoustic Focusing Cytometer (Life Technologies). For Cy3 single stain compensation

control we used cells isolated from the bone marrow. Proliferation rate was determined as the percentage of EdU^+ cells from the specific cell population.

p38 MAPK activity

p38 MAPK activity was assessed by quantifying phospho-p38 MAPK expression levels. *KO* and *floxed* female and male mice were intraperitoneally injected with 3 mg/kg LPS (O111:B4, Sigma). 24 h after, mice were deeply anesthetized and spleens were isolated, cut into smaller pieces in ice cold HBSS, and enzymatically digested for 20 min at 37^0C. Digested tissue was passed through a 70 µm cell strainer into 50 ml falcon tubes using the backside of 1 ml syringe. Cells were pelleted by centrifugation at 350 x g at 4^0C for 5 min and resuspended in ice cold 1 ml RBC lysis buffer. After washing and centrifugation, cells were resuspended in MACS buffer (PBS with 0.5% BSA and 2 mM EDTA) and counted using hematocytometer. After centrifugation, cells were resuspended and incubated in MACS buffer containing Fc blocker and CD11c MicroBeads (Miltenyi Biotec) according to manufacturer instruction. $CD11c^+$ cells were isolated using LS columns (Miltenyi Biotec, Cat# 130-108-338), pelleted and processed for staining. After Fc receptor blocking with CD16/CD32 antibody (BD Pharmingen), cells were stained with fluorophore-conjugated antibodies CD11b BV605 (1:200, clone M1/70, Biolegend) and CD11c APC (1:100, clone N418, Biolegend) on ice for 30-60 min. After washing, cells were incubated with dead cell dye Zombie red (1:1000 in PBS, Biolegend) for 15 min on ice. Cells were fixed for 15 min on ice using BD Cytofix/Cytoperm reagent. After washing with BD Perm/Wash, cells were incubated overnight with phospho-p38 MAPK PE (Thr180/Tyr182 (3D7), 1:50, Cell Signaling). Cells were analyzed on Attune NxT Acoustic Focusing Cytometer (Life Technologies). Unstained cells, single stain controls, stained AbC Total Antibody Compensation beads and isotype controls were used for each experiment. Acquired data were analyzed using FlowJo software (TreeStar).

RNA isolation and qPCR

RNA transcription levels of CCL2 in the lumbar spinal cord was analyzed using qPCR as described earlier (Chechneva *et al.*, 2011). Briefly, mice were anesthetized and transcardially perfused with ice cold PBS. Lumbar spinal cords were dissected and stored separately in liquid nitrogen. Total RNA was isolated from spinal cord tissue using Direct-zol RNA MiniPrep Kit (Zymo Research) following the manufacturer protocol. RNA at purity $OD_{260/280}$ ratio between 1.8 and 2.0 was reverse-transcribed to cDNA using Multiscribe reverse transcriptase (Applied Biosystems). TaqMan gene expression assay (Applied Biosystems) was used for *CCL2* (Mm00441242_m1). All experimental samples were normalized to the expression level of *GAPDH* (4352339E Applied Biosystems). Relative quantification of fold-change was performed by applying the $2^{-\Delta\Delta}$CT method and comparing Cp values of individual mice (Livak and Schmittgen, 2001).

Statistics

Statistical analysis was performed using GraphPad Prism 7.5. The numbers of animals per group used for each study are shown in the figures as individual dots or indicated in the figure legends. EAE clinical scores were pooled from four independent EAE experiments and evaluated for statistical significance using Two-way ANOVA with Sidak's multiple comparisons test. One-way ANOVA with Tukey's post hoc test was used to analyze EAE data shown in Table 1. Two group experiments were analyzed using Student's t-test. Experiments with three and more groups were analyzed using One-way ANOVA with Tukey's post hoc test. In all figures, data are represented as mean ± s.e.m. In all cases, probability values less than 0.05 were considered statistically significant. Images were assembled using Adobe Illustrator CC.

Results

Reduction in CD11c$^+$ microglia and dispersed parenchymal infiltration accompany the transition to EAE progression

EAE in C57BL/6 WT mice induced with MOG_{35-55} emulsion prepared by sonication results in severe clinical phenotype with continuous paralysis throughout disease course (score 3.5 – 4.5) (Chechneva *et al.*, 2011). We found that EAE induction using MOG_{35-55} emulsion prepared by syringe homogenization rather than sonication results in severe phenotype in 31% of cases. In addition, we observed mild non-progressive phenotype in 42% of cases and initially mild phenotype with progression around 30 days post immunization (dpi) in 27% of cases (Fig. 1A). Mild EAE was defined by chronic mild clinical symptoms, ranging from loss of tail tone to abnormal gait/paresis (maximum score 3) throughout EAE course. EAE progression was identified by transition from mild to severe disease around 30 dpi with an acute increase in clinical score by 1-2.5 points.

To define pathological features of EAE progression, we compared immune cell infiltration at EAE peak, EAE progression, and at 30 days of mild and severe EAE. Histological analysis revealed a distinctive dispersed coalescent infiltration of the spinal cord white matter at EAE progression compared to compact focal infiltrates found at EAE peak (Fig. 1B). A diffuse scattering of immune cells in the parenchyma with lower density than at EAE progression was observed in chronic severe EAE. In mild EAE, immune cells were concentrated at perivascular areas outside the CNS parenchyma (Fig. 1B). We characterized immune cell infiltrates in the CNS using flow cytometry. Increase in T_H1 and T_H17 effector cell populations was evident at EAE progression compared to mild and severe EAE (Supplementary Fig. 1A-D). The numbers of CD45$^+$ cells (Fig. 2A, F), including neutrophils (Fig. 2B, G), macrophages/monocytes (Fig. 2C, H) and CD11c$^+$ cells (Fig. 2D, J), were increased at EAE peak compared to all other groups. In the chronic phase the numbers of neutrophils, macrophages/monocytes and CD11c$^+$ cells were increased at EAE progression compared to mild and

severe EAE (Fig. 2B-D, G-H, J). We found no differences in $CD11b^{+}CD45^{lo}$ microglia numbers between EAE groups (Fig. 2C, I).

$CD11c^{+}$ cells are involved in re-activation of myelin reactive T cells and EAE progression (Giles *et al.*, 2018a; Greter *et al.*, 2005; Mundt *et al.*, 2019). We differentiated $CD11c^{+}$ cells in three populations by expression of CD45 and CD11b: 1) $CD11c^{+}CD11b^{-}CD45^{hi}$ or cDC, 2) $CD11c^{+}CD11b^{+}CD45^{hi}$ or moDC, and 3) $CD11c^{+}CD11b^{+}CD45^{lo}$ or $CD11c^{+}$ microglia (Fig. 2E). cDC (Fig. 2E, K) and moDC (Fig. 2E, L) numbers were elevated at EAE peak and EAE progression compared to mild and severe EAE. Strikingly, the population of $CD11c^{+}$ microglia was reduced at EAE progression compared to all groups (Fig. 2E, M). The proportions of $CD11c^{+}$ microglia among $CD11c^{+}$ cells were reduced at EAE peak and EAE progression compared to mild and severe EAE (Supplementary Fig. 1G). Gating on $CD11c^{+}$ microglia from the pool of $CD11b^{+}CD45^{lo}$ populations resulted in a similar outcome (Supplementary Fig. 1E-F). No sex-dependent differences in immune cell populations were found in all experimental conditions. We conclude that $CD11c^{+}$ microglia population is reduced during dispersed coalescent infiltration at EAE progression.

Knockout of *p38α* reduces $CD11c^{+}$ microglia proliferation in female mice

Microglia populations are maintained by self-renewal (Huang *et al.*, 2018). Microglia proliferation is dependent on p38 MAPK signaling (Merighi *et al.*, 2017). We examined the proliferation rate of $CD11c^{+}$ microglia in mice with CD11c promoter-driven knockout of *p38α* (*KO*) during immune response. MOG-immunized *floxed* control and *KO* mice without EAE symptoms had an increased number of CNS associated $CD45^{+}$ immune cells at 30 dpi (Supplementary Fig. 2A). Under this condition, the numbers and proliferation rates of cDC, macrophages/monocytes and total microglia were not affected by knockout of *p38α* in $CD11c^{+}$ cells (Fig. 3A, B, E, Supplementary Fig. 2B-D). moDC were increased in numbers without differences in proliferation rate in *KO* males compared to other groups (Fig. 3A, C, F). Strikingly, the numbers and proliferation rates of $CD11c^{+}$ microglia were reduced in female *KO* mice compared to *KO* males (Fig. 3A, D, G). There was no difference in

CD11c$^+$ microglia numbers and proliferation rates under steady-state condition between groups (Supplementary Fig. 2E-F). To confirm efficient *p38α* knockout, reduced expression of the activated form of p38 MAPK, phospho-p38 MAPK, was found in CD11c$^+$ splenocytes in *KO* female and *KO* male mice after LPS stimulation compared to *floxed* control (Supplementary Fig. 3A-B). We conclude that under immune stimulation CD11c$^+$ microglia proliferation is reduced in female mice with *p38α* knockout.

Knockout of *p38α* promotes sex-dependent transition of chronic mild EAE to clinical progression

We followed EAE clinical symptoms for 60 days in *floxed* control and *KO* female and male mice immunized with MOG_{35-55} prepared by sonication. *KO* mice were protected and initially displayed mild EAE, as reported earlier (Huang *et al.*, 2012; Krementsov *et al.*, 2014). EAE onset and peak were delayed in *KO* females compared to *KO* males (Fig. 4A, Table 1). *Floxed* control mice developed severe disease with no sex differences (Fig. 4A, Table 1). Notably, around 30 dpi, 58% of *KO* females underwent clinical progression (Fig. 4A, Table 1). No progression of EAE clinical symptoms was observed in *KO* males (Fig. 4A, Table 1).

We examined chronic EAE pathology in the lumbar spinal cord using LFB & Cresyl Violet staining. In *floxed* control mice we found infiltration and demyelination with no sex differences (Fig. 4B-C). *KO* males displayed clusters of immune cells accumulated at perivascular areas and meninges (Fig. 4B-C). *KO* females that did not develop EAE progression showed minimal immune cell parenchymal and perivascular presence with no demyelination (Fig. 4B-C). In contrast, progressed *KO* females showed dispersed infiltration and demyelination throughout the white matter (Fig. 4B-C). We further characterized immune cell infiltrates in the brain and spinal cord of *KO* mice. In progressed *KO* females, CD4$^+$ cells, were localized within white matter parenchyma (Fig. 4D). In *KO* males, CD4$^+$ cells formed clusters at perivascular sites with rare parenchymal presence (Fig. 4E). The numbers of

parenchymal $CD4^+$ T cells in the lumbar spinal cord were increased in progressed *KO* females compared to *KO* males (Fig. 4F). Flow cytometry analysis showed increase in $CD3^+$ T cells (Fig. 4G) that primarily included INF-γ^+ T_H1 cells (Supplementary Fig. 4A). Macrophages/monocytes displayed similar infiltration patterns where $Iba1^+$ or $lectin^+$ cells were scattered throughout white matter parenchyma in progressed *KO* females (Fig. 5A, C), but clustered along perivascular spaces and meninges in *KO* males (Fig. 5B, D). Immunostaining and FACS showed increase in $CD45^+$ cells in the brain and spinal cord during EAE progression in *KO* females (Fig. 5E-G, J). $CD45^+$ cells included $Ly6G^+$ neutrophils (Fig. 5H, K) and $CD11b^+CD45^{hi}$ macrophages/monocytes (Fig. 5I, L). There were no differences in the numbers of $CD11b^+CD45^{lo}$ microglia between groups (Fig. 5I, M). To visualize $CD11c^+$ cells in the spinal cord, we used expression of eGFP under the CD11c promoter (Merad *et al.*, 2013; Prodinger *et al.*, 2011). In progressed *KO* females, $eGFP^+CD11b^+$ moDC were localized in the white matter parenchyma (Fig. 6A). In *KO* males, moDC were found at the perivascular areas and meninges (Fig. 6B), while $eGFP^+CD11b^+$ microglia were morphologically distinct from moDC and found in the parenchyma (Fig. 6B, arrows). FACS analysis showed an increased number of $CD11c^+$ cells in the brain and spinal cord of progressed *KO* females (Fig. 6C-D), which was driven by an increase in moDC (Fig. 6F-G). $CD11c^+$ microglia were significantly reduced in progressed *KO* females compared to *floxed* control mice and *KO* males (Fig. 6H). Gating on $CD11c^+$ microglia from the pool of $CD11b^+CD45^{lo}$ microglia resulted in a similar outcome (Supplementary Fig. 5A-B). We conclude that p38α-dependent reduction in $CD11c^+$ microglia promotes transition to EAE progression in *KO* females.

$CD11c^+$ microglia contact glia limitans in *KO* males

Glia limitans astrocytic endfeet control immune cell parenchymal infiltration (Quintana, 2017). We examined $CD11c^+$ microglia localization in relation to astrocytes. In progressed *KO* females, we found disorganized hypertrophic astrocyte processes surrounded by moDC (Fig. 7A). $CD11c^+$ microglia were not morphologically distinguishable from moDC. In *KO* males, glia limitans and

astrocyte processes that extended from meninges through the white matter parenchyma were clearly defined (Fig. 7B). We identified DC-like CD11c$^+$ microglia with stellate thick processes located within spinal cord parenchyma of *KO* male mice (Fig. 6B, arrowhead). DC-like CD11c$^+$ microglia were localized in close contact with glia limitans (Fig. 7B) and astrocyte processes (Fig. 7C). Levels of CCL2, a macrophage/monocytes attracting chemokine, were decreased in *KO* male compared to progressed *KO* female mice (Fig. 7D-E). CCL2 mRNA levels were also decreased in the spinal cord of *KO* males (Fig. 7F). We conclude that CD11c$^+$ microglia regulate parenchymal infiltration through interaction with glia limitans astrocyte endfeet.

Discussion

Like MS, EAE is a complex pathological condition, characterized by high variability of clinical symptoms. EAE allows to model a variety of clinical mechanisms featured in MS. Our previously described EAE model of MOG_{35-55} prepared by sonication consistently causes severe EAE in WT mice (Chechneva *et al.*, 2011). Changes in MOG epitope and/or Mycobacterium tuberculosis biochemical composition by sonication may explain an enhanced immune response to immunization in this model (Adelmann *et al.*, 1995). We newly found that syringe emulsification of MOG_{35-55}, results in more variable outcome in WT mice that we classified into three distinct EAE phenotypes: mild, severe and progressive EAE. We show that around 30 dpi, spontaneous EAE progression occurs in ~40% of mice that initially develop mild disease. A similar course of EAE has been reported in non-obese diabetic mice (Basso *et al.*, 2008; Encinas *et al.*, 1999; Tanabe *et al.*, 2019). However, non-obese diabetic mice gradually develop hyperglycemia at 12-15 weeks of age that alters cellular and molecular mechanism of EAE and limits its use as a model of MS (Mathews *et al.*, 2015). We identified dispersed coalescent infiltration at EAE progression and a comparable infiltration pattern with lesser cell density at chronic severe EAE, which suggests that diffuse CNS infiltration is a hallmark of irreversible disability in EAE.

By comparing immune cell compositions in different EAE phenotypes, we identified a link between reduction in CD11c$^+$ microglia population, dispersed parenchymal infiltration and transition from chronic mild to severe EAE. Using a transgenic mouse model where deletion of *p38α* reduced CD11c$^+$ microglia proliferation in female mice, we determined a critical role of CD11c$^+$ microglia in controlling parenchymal infiltration and EAE progression. Our findings demonstrate a novel neuroprotective role of CD11c$^+$ microglia in EAE, in line with a recent study, where depletion of microglia with antagonist of colony-stimulated factor 1 receptor, PLX3397, resulted in expansion of CD4$^+$ T cells and exacerbation of EAE in non-obese diabetic mice (Tanabe *et al.*, 2019). This study, however, did not differentiate the role of CD11c$^+$ microglia from other microglia subtypes.

How CD11c$^+$ microglia control immune cell infiltration is still unclear. Our data suggest a direct interaction with astrocytes. Glia limitans astrocytic endfeet surround blood-brain barrier endothelial cells and form a physical border between perivascular space and CNS parenchyma (Quintana, 2017). Reactive astrocytes control CNS infiltration by expression of macrophages/monocytes attracting chemokine, CCL2 (Dogan *et al.*, 2008; Moreno *et al.*, 2014). In the white matter of *KO* males, where parenchymal infiltration was limited, DC-like CD11c$^+$ microglia with stellate thick processes localized in close contact with glia limitans and astrocyte processes. The presence of DC-like CD11c$^+$ microglia at the glia limitans has been reported in the brain, spinal cord and optic nerve parenchyma of healthy mice, suggesting their role in astrocyte glia limitans organization (Prodinger *et al.*, 2011). We found that the presence of CD11c$^+$ microglia at astrocyte endfeet correlated with reduced CCL2 expression in astrocytes and restricted immune cell infiltration. The detailed mechanism of CD11c$^+$ microglia and astrocytes cross talk and its specific role in CNS infiltration remains to be determined.

p38 MAPK signaling is involved in hormone-dependent sexual dimorphism of the immune response. In microglia, p38 MAPK signaling was identified as a cause of neuropathic and inflammatory pain in males in chronic constriction injury and mechanical allodynia (Sorge *et al.*, 2015; Taves *et al.*, 2016). Testosterone-dependent increase in p38 MAPK phosphorylation in splenic and peritoneal

macrophages was reported in male mice after trauma-hemorrhage (Angele *et al.*, 2003). Pharmacological inhibition of p38 MAPK signaling protected female mice at EAE acute phase (Krementsov *et al.*, 2014). Knockout of *p38α* in CD11c$^+$ cells protected both, female and male mice, at the initial EAE phase (Huang *et al.*, 2012; Krementsov *et al.*, 2014). We found a delay in EAE onset and peak in female mice with knockout of *p38α* in CD11c$^+$ cells, suggesting a sex-dependent response of cDC and moDC, which may explain the fraction of *KO* females with chronic mild EAE, due to inefficient T-cell priming and/or reduced moDC infiltration. In support, a reduction of EAE clinical symptoms was found in female but not male mice with knockout of *p38α* in LyzM$^+$ myeloid cells, including moDC (Krementsov *et al.*, 2014). The diverse functions of p38α signaling depending on the cell type and sex may explain the reason why many of p38 MAPK inhibitors failed to fulfill their expectations in clinical trials (Goldstein *et al.*, 2010; Krementsov *et al.*, 2013).

Conclusions: Our findings demonstrate a novel neuroprotective function of CD11c$^+$ microglia in the context of chronic neuroinflammation. We identified a sex-dependent mechanism of p38α signaling in CD11c$^+$ microglia and uncovered a novel regulatory role of CD11c$^+$ microglia in the clinical progression of chronic autoimmune demyelination. Further studies to explore CD11c$^+$ microglia populations during chronic neuroinflammation and identify the cause of CD11c$^+$ microglia reduction leading to disease progression are warranted. Ultimately, modulation of CD11c$^+$ microglia might provide us a unique therapeutic tool for future treatment of CNS immune disorders.

References

Adelmann, M., Wood, J., Benzel, I., Fiori, P., Lassmann, H., Matthieu, J.M., Gardinier, M.V., Dornmair, K., Linington, C., 1995. The N-terminal domain of the myelin oligodendrocyte glycoprotein (MOG) induces acute demyelinating experimental autoimmune encephalomyelitis in the Lewis rat. *J Neuroimmunol* 63**,** 17-27.

Angele, M.K., Nitsch, S., Knoferl, M.W., Ayala, A., Angele, P., Schildberg, F.W., Jauch, K.W., Chaudry, I.H., 2003. Sex-specific p38 MAP kinase activation following trauma-hemorrhage: involvement of testosterone and estradiol. *Am J Physiol Endocrinol Metab* 285**,** E189-196.

Baecher-Allan, C., Kaskow, B.J., Weiner, H.L., 2018. Multiple Sclerosis: Mechanisms and Immunotherapy. *Neuron* 97**,** 742-768.

Basso, A.S., Frenkel, D., Quintana, F.J., Costa-Pinto, F.A., Petrovic-Stojkovic, S., Puckett, L., Monsonego, A., Bar-Shir, A., Engel, Y., Gozin, M., Weiner, H.L., 2008. Reversal of axonal loss and disability in a mouse model of progressive multiple sclerosis. *J Clin Invest* 118**,** 1532-1543.

Butovsky, O., Koronyo-Hamaoui, M., Kunis, G., Ophir, E., Landa, G., Cohen, H., Schwartz, M., 2006. Glatiramer acetate fights against Alzheimer's disease by inducing dendritic-like microglia expressing insulin-like growth factor 1. *Proceedings of the National Academy of Sciences of the United States of America* 103**,** 11784-11789.

Chechneva, O.V., Mayrhofer, F., Daugherty, D.J., Pleasure, D.E., Hong, J.S., Deng, W., 2011. Low dose dextromethorphan attenuates moderate experimental autoimmune encephalomyelitis by inhibiting NOX2 and reducing peripheral immune cells infiltration in the spinal cord. *Neurobiol Dis* 44**,** 63-72.

Coret, F., Perez-Miralles, F.C., Gascon, F., Alcala, C., Navarre, A., Bernad, A., Bosca, I., Escutia, M., Gil-Perotin, S., Casanova, B., 2018. Onset of secondary progressive multiple sclerosis is not influenced by current relapsing multiple sclerosis therapies. *Mult Scler J Exp Transl Clin* 4**,** 2055217318783347.

Di Mitri, D., Sambucci, M., Loiarro, M., De Bardi, M., Volpe, E., Cencioni, M.T., Gasperini, C., Centonze, D., Sette, C., Akbar, A.N., Borsellino, G., Battistini, L., 2015. The p38 mitogen-activated protein kinase cascade modulates T helper type 17 differentiation and functionality in multiple sclerosis. *Immunology* 146**,** 251-263.

Dogan, R.N., Elhofy, A., Karpus, W.J., 2008. Production of CCL2 by central nervous system cells regulates development of murine experimental autoimmune encephalomyelitis through the recruitment of TNF- and iNOS-expressing macrophages and myeloid dendritic cells. *J Immunol* 180**,** 7376-7384.

Encinas, J.A., Wicker, L.S., Peterson, L.B., Mukasa, A., Teuscher, C., Sobel, R., Weiner, H.L., Seidman, C.E., Seidman, J.G., Kuchroo, V.K., 1999. QTL influencing autoimmune diabetes and encephalomyelitis map to a 0.15-cM region containing Il2. *Nat Genet* 21**,** 158-160.

Fischer, H.G., Reichmann, G., 2001. Brain dendritic cells and macrophages/microglia in central nervous system inflammation. *J Immunol* 166**,** 2717-2726.

Ford, A.L., Goodsall, A.L., Hickey, W.F., Sedgwick, J.D., 1995. Normal adult ramified microglia separated from other central nervous system macrophages by flow cytometric sorting. Phenotypic differences defined and direct ex vivo antigen presentation to myelin basic protein-reactive CD4+ T cells compared. *J Immunol* 154**,** 4309-4321.

Giles, D.A., Duncker, P.C., Wilkinson, N.M., Washnock-Schmid, J.M., Segal, B.M., 2018a. CNS-resident classical DCs play a critical role in CNS autoimmune disease. *J Clin Invest* 128**,** 5322-5334.

Giles, D.A., Washnock-Schmid, J.M., Duncker, P.C., Dahlawi, S., Ponath, G., Pitt, D., Segal, B.M., 2018b. Myeloid cell plasticity in the evolution of central nervous system autoimmunity. *Ann Neurol* 83**,** 131-141.

Goldstein, D.M., Kuglstatter, A., Lou, Y., Soth, M.J., 2010. Selective p38alpha inhibitors clinically evaluated for the treatment of chronic inflammatory disorders. *J Med Chem* 53**,** 2345-2353.

Greter, M., Heppner, F.L., Lemos, M.P., Odermatt, B.M., Goebels, N., Laufer, T., Noelle, R.J., Becher, B., 2005. Dendritic cells permit immune invasion of the CNS in an animal model of multiple sclerosis. *Nat Med* 11**,** 328-334.

Huang, G., Wang, Y., Vogel, P., Kanneganti, T.D., Otsu, K., Chi, H., 2012. Signaling via the kinase p38alpha programs dendritic cells to drive TH17 differentiation and autoimmune inflammation. *Nat Immunol* 13**,** 152-161.

Huang, Y., Xu, Z., Xiong, S., Sun, F., Qin, G., Hu, G., Wang, J., Zhao, L., Liang, Y.X., Wu, T., Lu, Z., Humayun, M.S., So, K.F., Pan, Y., Li, N., Yuan, T.F., Rao, Y., Peng, B., 2018. Repopulated microglia are solely derived from the proliferation of residual microglia after acute depletion. *Nat Neurosci* 21**,** 530-540.

Kamphuis, W., Kooijman, L., Schetters, S., Orre, M., Hol, E.M., 2016. Transcriptional profiling of CD11c-positive microglia accumulating around amyloid plaques in a mouse model for Alzheimer's disease. *Biochim Biophys Acta* 1862**,** 1847-1860.

King, I.L., Dickendesher, T.L., Segal, B.M., 2009. Circulating Ly-6C+ myeloid precursors migrate to the CNS and play a pathogenic role during autoimmune demyelinating disease. *Blood* 113**,** 3190-3197.

Krementsov, D.N., Noubade, R., Dragon, J.A., Otsu, K., Rincon, M., Teuscher, C., 2014. Sex-specific control of central nervous system autoimmunity by p38 mitogen-activated protein kinase signaling in myeloid cells. *Ann Neurol* 75**,** 50-66.

Krementsov, D.N., Thornton, T.M., Teuscher, C., Rincon, M., 2013. The emerging role of p38 mitogen-activated protein kinase in multiple sclerosis and its models. *Mol Cell Biol* 33**,** 3728-3734.

Livak, K.J., Schmittgen, T.D., 2001. Analysis of relative gene expression data using real-time quantitative PCR and the 2(-Delta Delta C(T)) Method. *Methods* 25**,** 402-408.

Lo, U., Selvaraj, V., Plane, J.M., Chechneva, O.V., Otsu, K., Deng, W., 2014. p38alpha (MAPK14) critically regulates the immunological response and the production of specific cytokines and chemokines in astrocytes. *Sci Rep* 4**,** 7405.

Lock, C., Hermans, G., Pedotti, R., Brendolan, A., Schadt, E., Garren, H., Langer-Gould, A., Strober, S., Cannella, B., Allard, J., Klonowski, P., Austin, A., Lad, N., Kaminski, N., Galli, S.J., Oksenberg, J.R., Raine, C.S., Heller, R., Steinman, L., 2002. Gene-microarray analysis of multiple sclerosis lesions yields new targets validated in autoimmune encephalomyelitis. *Nat Med* 8**,** 500-508.

Mathews, C.E., Xue, S., Posgai, A., Lightfoot, Y.L., Li, X., Lin, A., Wasserfall, C., Haller, M.J., Schatz, D., Atkinson, M.A., 2015. Acute Versus Progressive Onset of Diabetes in NOD Mice: Potential Implications for Therapeutic Interventions in Type 1 Diabetes. *Diabetes* 64**,** 3885-3890.

Merad, M., Sathe, P., Helft, J., Miller, J., Mortha, A., 2013. The dendritic cell lineage: ontogeny and function of dendritic cells and their subsets in the steady state and the inflamed setting. *Annu Rev Immunol* 31**,** 563-604.

Merighi, S., Bencivenni, S., Vincenzi, F., Varani, K., Borea, P.A., Gessi, S., 2017. A2B adenosine receptors stimulate IL-6 production in primary murine microglia through p38 MAPK kinase pathway. *Pharmacol Res* 117**,** 9-19.

Miller, S.D., McMahon, E.J., Schreiner, B., Bailey, S.L., 2007. Antigen presentation in the CNS by myeloid dendritic cells drives progression of relapsing experimental autoimmune encephalomyelitis. *Ann N Y Acad Sci* 1103**,** 179-191.

Moreno, M., Bannerman, P., Ma, J., Guo, F., Miers, L., Soulika, A.M., Pleasure, D., 2014. Conditional ablation of astroglial CCL2 suppresses CNS accumulation of M1 macrophages and preserves axons in mice with MOG peptide EAE. *J Neurosci* 34**,** 8175-8185.

Mundt, S., Mrdjen, D., Utz, S.G., Greter, M., Schreiner, B., Becher, B., 2019. Conventional DCs sample and present myelin antigens in the healthy CNS and allow parenchymal T cell entry to initiate neuroinflammation. *Sci Immunol* 4.

Prodinger, C., Bunse, J., Kruger, M., Schiefenhovel, F., Brandt, C., Laman, J.D., Greter, M., Immig, K., Heppner, F., Becher, B., Bechmann, I., 2011. CD11c-expressing cells reside in the juxtavascular parenchyma and extend processes into the glia limitans of the mouse nervous system. *Acta Neuropathol* 121**,** 445-458.

Quintana, F.J., 2017. Astrocytes to the rescue! Glia limitans astrocytic endfeet control CNS inflammation. *J Clin Invest* 127**,** 2897-2899.

Sato-Hashimoto, M., Nozu, T., Toriba, R., Horikoshi, A., Akaike, M., Kawamoto, K., Hirose, A., Hayashi, Y., Nagai, H., Shimizu, W., Saiki, A., Ishikawa, T., Elhanbly, R., Kotani, T., Murata, Y., Saito, Y., Naruse, M., Shibasaki, K., Oldenborg, P.A., Jung, S., Matozaki, T., Fukazawa, Y., Ohnishi, H., 2019. Microglial SIRPalpha regulates the emergence of CD11c(+) microglia and demyelination damage in white matter. *Elife* 8.

Serafini, B., Columba-Cabezas, S., Di Rosa, F., Aloisi, F., 2000. Intracerebral recruitment and maturation of dendritic cells in the onset and progression of experimental autoimmune encephalomyelitis. *Am J Pathol* 157**,** 1991-2002.

Shi, L.Z., Wang, R., Huang, G., Vogel, P., Neale, G., Green, D.R., Chi, H., 2011. HIF1alpha-dependent glycolytic pathway orchestrates a metabolic checkpoint for the differentiation of TH17 and Treg cells. *J Exp Med* 208**,** 1367-1376.

Sorge, R.E., Mapplebeck, J.C., Rosen, S., Beggs, S., Taves, S., Alexander, J.K., Martin, L.J., Austin, J.S., Sotocinal, S.G., Chen, D., Yang, M., Shi, X.Q., Huang, H., Pillon, N.J., Bilan, P.J., Tu, Y., Klip, A., Ji, R.R., Zhang, J., Salter, M.W., Mogil, J.S., 2015. Different immune cells mediate mechanical pain hypersensitivity in male and female mice. *Nat Neurosci* 18**,** 1081-1083.

Tanabe, S., Saitoh, S., Miyajima, H., Itokazu, T., Yamashita, T., 2019. Microglia suppress the secondary progression of autoimmune encephalomyelitis. *Glia* 67**,** 1694-1704.

Taves, S., Berta, T., Liu, D.L., Gan, S., Chen, G., Kim, Y.H., Van de Ven, T., Laufer, S., Ji, R.R., 2016. Spinal inhibition of p38 MAP kinase reduces inflammatory and neuropathic pain in male but not female mice: Sex-dependent microglial signaling in the spinal cord. *Brain, behavior, and immunity* 55**,** 70-81.

Trapp, B.D., Bo, L., Mork, S., Chang, A., 1999. Pathogenesis of tissue injury in MS lesions. *J Neuroimmunol* 98**,** 49-56.

Wlodarczyk, A., Benmamar-Badel, A., Cedile, O., Jensen, K.N., Kramer, I., Elsborg, N.B., Owens, T., 2018. CSF1R Stimulation Promotes Increased Neuroprotection by CD11c+ Microglia in EAE. *Front Cell Neurosci* 12**,** 523.

Wlodarczyk, A., Cedile, O., Jensen, K.N., Jasson, A., Mony, J.T., Khorooshi, R., Owens, T., 2015. Pathologic and Protective Roles for Microglial Subsets and Bone Marrow- and Blood-Derived Myeloid Cells in Central Nervous System Inflammation. *Front Immunol* 6**,** 463.

Zarubin, T., Han, J., 2005. Activation and signaling of the p38 MAP kinase pathway. *Cell Res* 15**,** 11-18.

Zhang, T., Shirani, A., Zhao, Y., Karim, M.E., Gustafson, P., Petkau, J., Evans, C., Kingwell, E., van der Kop, M., Zhu, F., Oger, J., Tremlett, H., Neurologists, B.M.C., 2015. Beta-interferon exposure and onset of secondary progressive multiple sclerosis. *Eur J Neurol* 22**,** 990-1000.

Author contributions: O.V.C. and F.M. designed the research, performed experiments, interpreted the data, wrote and edited the manuscript. Z.D., A.Z., D.J.D., and A.M.H. performed experiments. P.B., D.P., A.S., and W.D. interpreted the data and edited the manuscript.

Conflict of interest: The authors have declared that no conflict of interest exists.

Funding: This work was in parts supported by grants from National Institutes of Health (R01HD087566 to W.D.) and Shriners Hospital for Children (87310 to O.C.).

Table 1. Clinical assessment of EAE in *p38α floxed* and CD11c promoter-driven *p38α KO* female and male mice

Group	n	Onset	Max severity 1st peak	Mean score d26	Mean score d32	Max severity d29-d60	Score at d60	Survival
floxed males	41	11.2 ± 0.2	4.2 ± 0.1***	3.2 ± 0.2***	3.4 ± 0.2***	3.9 ± 0.1***	3.7 ± 0.2***	90.2%
floxed females	32	12.4 ± 0.4**	4.0 ± 0.1	3.2 ± 0.2	3.3 ± 0.2	3.7 ± 0.2	3.4 ± 0.2	90.6%
KO males	47	12.2 ± 0.3	3.3 ± 0.1	2.2 ± 0.2	2.1 ± 0.2	2.7 ± 0.2	2.1 ± 0.2	95.7%
progressive KO females	23	14.6 ± 0.8###	3.6 ± 0.2	2.6 ± 0.3	3.5 ± 0.2###	4.1 ± 0.1###	3.7 ± 0.2###	91.3%

Data are the mean ± s.e.m. *P<0.05, **P<0.01, ***P<0.001, comparing between same sex *floxed* and *KO* mice. #P<0.05, ###P<0.01, comparing between females and males of the same genotype. P values were determined by One-way ANOVA with Tukey's post hoc test.

Figures

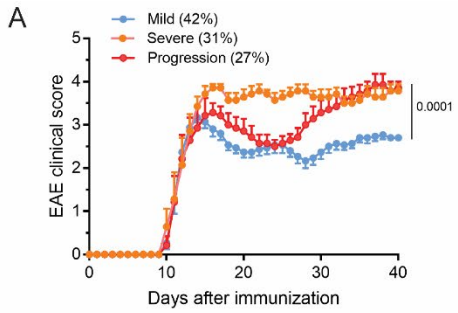

EAE type	All mice	Males	Females
Mild	23/55 (42%)	14/33 (43%)	9/22 (41%)
Severe	17/55 (31%)	9/33 (27%)	8/22 (36%)
Progression	15/55 (27%)	10/33 (30%)	5/22 (23%)

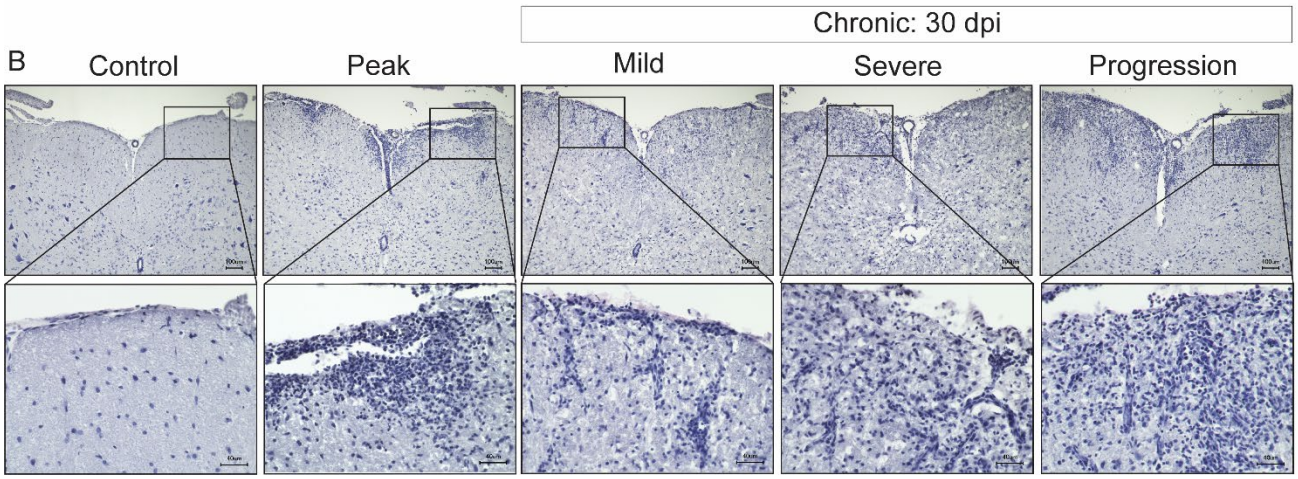

Fig. 1. Diffuse parenchymal infiltration drives EAE progression.
(A) EAE was induced in C57BL/6 mice with MOG_{35-55} prepared by syringe homogenization. Animals were grouped based on chronic EAE disease course: mild, severe or progression. (B) Representative images of H&E staining of the lumbar spinal cord in healthy control, at EAE peak, and in chronic mild, severe and progressive EAE. Scale bar 100 µm and 40 µm for insert. Data are representative of six independent experiments. Individual time points represent mean ± s.e.m. *P* values were determined by two-way ANOVA with Sidak's multiple comparisons test. dpi, days post immunization.

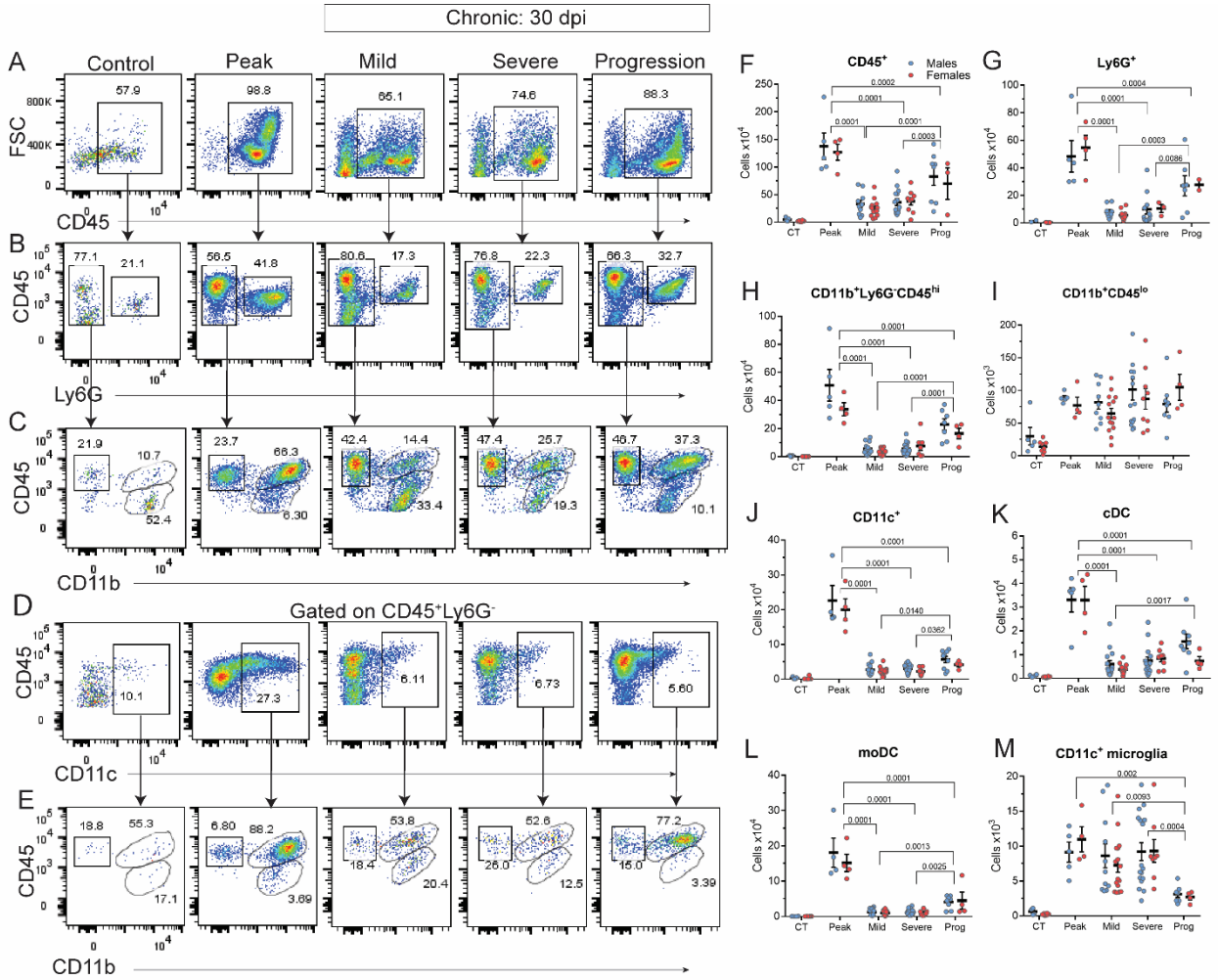

Fig. 2. Reduction in CD11c$^+$ microglia accompanies EAE progression.
EAE was induced in C57BL/6 mice with MOG$_{35-55}$ prepared by syringe homogenization. Isolated cells from the brain and spinal cord of healthy mice, at EAE peak, EAE progression and at 30 days of mild and severe EAE were analyzed using flow cytometry. (A) FACS analysis of CD45$^+$ cells. (B) FACS analysis of Ly6G$^+$ neutrophils. (C) FACS analysis of CD11b$^+$CD45^{hi}Ly6G$^-$ macrophages/monocytes and CD11b$^+$CD45^{lo} microglia. (D) FACS analysis of CD11c$^+$ cells. (E) Gating strategy to differentiate cDC, moDC and CD11c$^+$ microglia by expression of CD45 and CD11b. (F-M) Quantification of CD45$^+$ cells, Ly6G$^+$ neutrophils, CD11b$^+$CD45^{hi} macrophages/monocytes, CD11b$^+$CD45^{lo} microglia, CD11c$^+$ cells, cDC, moDC and CD11c$^+$ microglia. Data are representative of six independent experiments. Each point represents an individual animal. *P* values were determined by One-way ANOVA with Tukey's post hoc test. dpi, days post immunization.

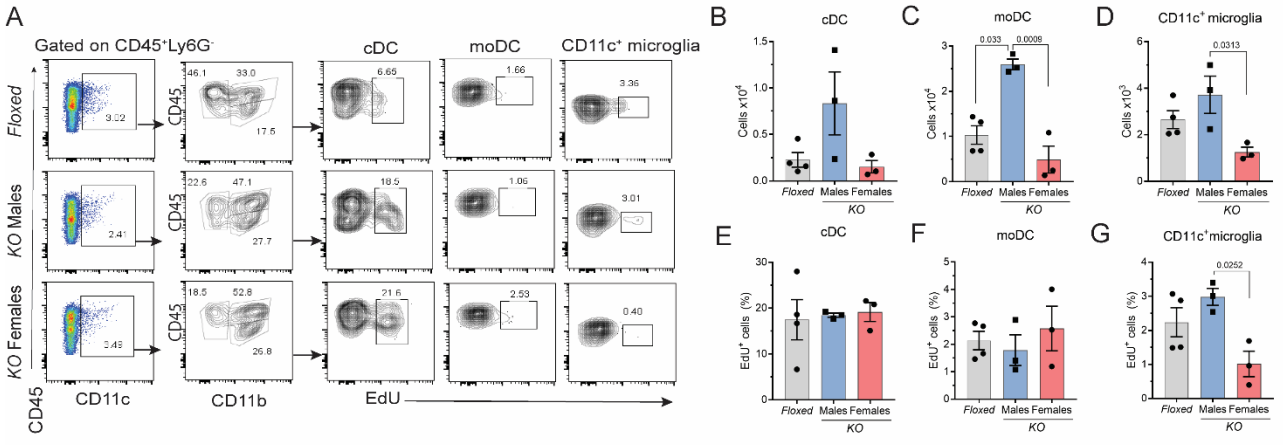

Fig. 3. Knockout of *p38α* reduces CD11c$^+$ microglia proliferation in female mice.
MOG-immunized *p38α floxed* control and CD11c promoter-driven *KO* female and male mice without EAE clinical symptoms were injected with 12 mg/kg EdU twice in 12 h interval at day 30 post immunization. EdU$^+$ cells were analyzed 24 h after first injection. (A) Gating strategy for CD11c$^+$EdU$^+$ cells isolated from the CNS. (B) Quantification of cDC. (C) Quantification of moDC. (D) Quantification of CD11c$^+$ microglia. (E-G) Proliferation response determined as percentage of EdU$^+$ cells for cDC, moDC and CD11c$^+$ microglia. Data are representative of two independent experiments. Each point represents an individual animal. *P* values were determined by One-way ANOVA with Tukey's post hoc test. *KO*, knockout.

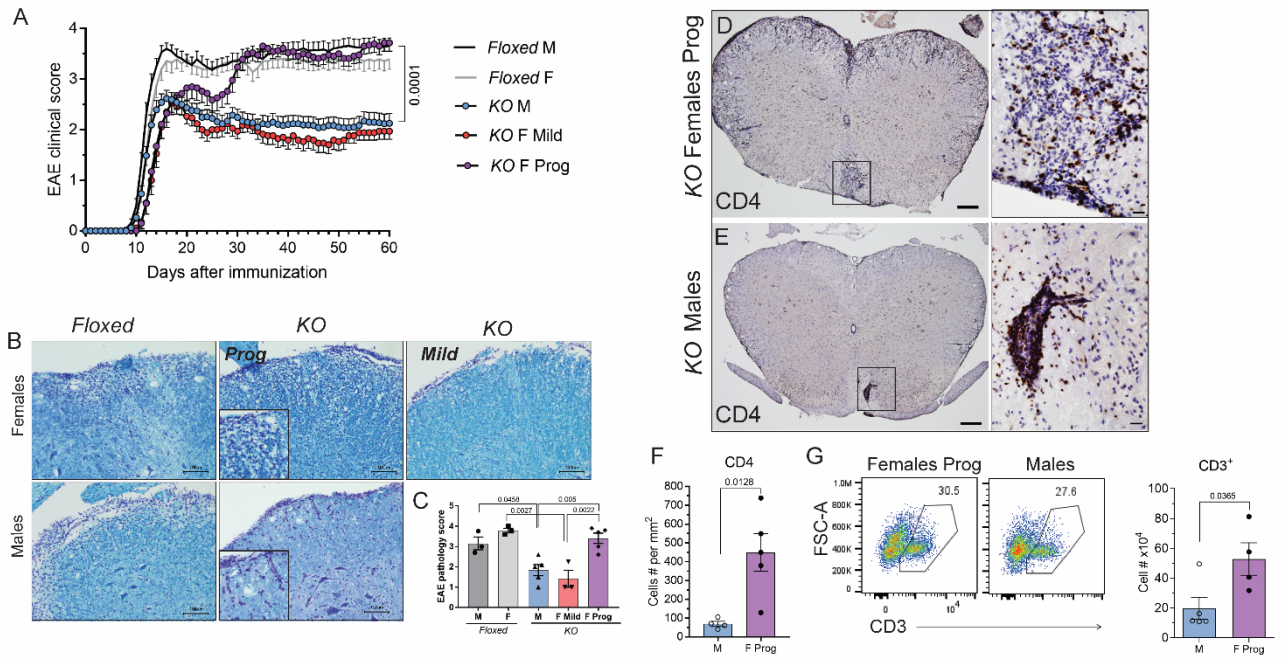

Fig. 4. Knockout of *p38α* in CD11c$^+$ cells promotes dispersed parenchymal infiltration and EAE progression in female mice.

p38α floxed control and CD11c promoter-driven *KO* female and male mice were immunized with MOG_{35-55} prepared by sonication to induce EAE. (A) EAE clinical scores were monitored daily through day 60 post immunization. Data are representative of four independent experiments with n = 41 for *floxed* males, n = 32 for *floxed* females, n = 47 for *KO* males, n = 23 for *KO* females with progression, and n = 17 for *KO* females with chronic mild EAE. *P* values were determined by two-way ANOVA with Sidak's multiple comparisons test; (B) Representative images of LFB staining of the lumbar spinal cord of *floxed* and *KO* male and female mice at chronic EAE phase. Scale bar 100 µm. (C) Pathological assessment of chronic EAE based on scoring the degree of infiltration and demyelination. Data are representative of two independent experiments. *P* values were determined by One-way ANOVA with Tukey's post hoc test. (D-E) Distribution of CD4$^+$ T cells in the lumbar spinal cord of *KO* male and progressed *KO* female mice. Note the differences of CD4$^+$ cell distribution in dorsal lumbar spinal cord (enlargements) between sexes. Scale bars 200 µm for D-E, 20 µm for enlargements. (F) Quantitative analysis of CD4$^+$ cells in the white matter parenchyma of the lumbar spinal cord of *KO* male and progressed *KO* female mice. (G) CD3$^+$ T cells analyzed by flow cytometry in the brain and spinal cord of *KO* male and progressed *KO* female mice. Data are representative of two independent experiments. *P* values were determined by Student's t-test. Each circle represents an individual mouse. F, females; *KO*, knockout; M, males; prog, progression.

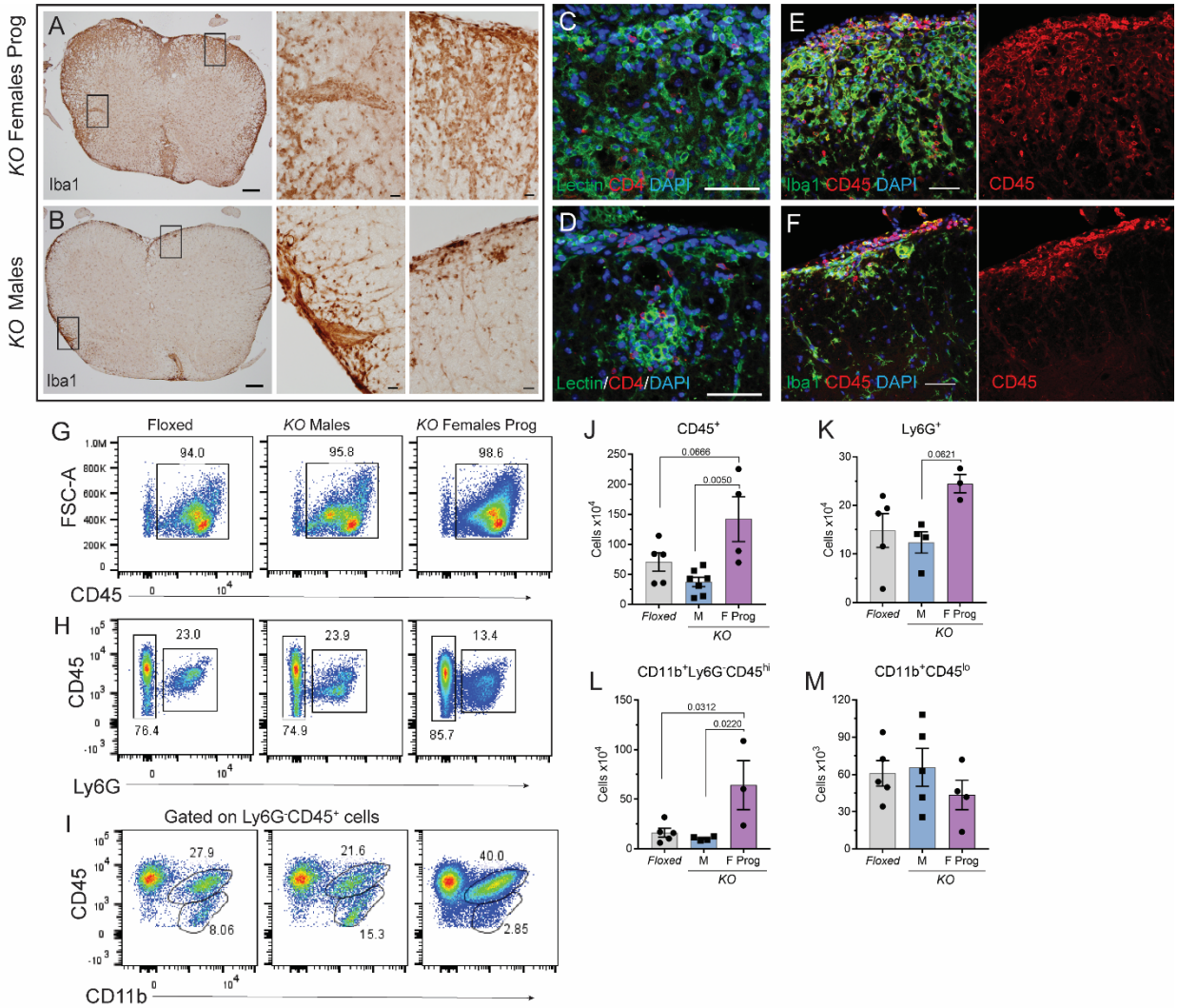

Fig. 5. Dispersed CNS infiltration of myeloid cells accompanies EAE progression in *p38α* knockout female mice.

(A-B) Iba1^{+} cells in the lateral and ventral (enlargements) lumbar spinal cord of *KO* male and progressed *KO* female mice at 30 dpi. (C-D) Infiltrating lectin^{+} macrophages/monocytes and CD4^{+} T cells in the ventral lumbar spinal cord at 30 dpi. (E-F) Infiltrating CD45^{+} cells in the ventral lumbar spinal cord at 30 dpi. (G-I) FACS analysis of CD45^{+} cells, Ly6G^{+} neutrophils, CD11b^{+}CD45^{hi} macrophages/monocytes and CD11b^{+}CD45^{lo} microglia isolated from the brain and spinal cord. (J-M) Quantification of CD45^{+} cells, Ly6G^{+} neutrophils, CD11b^{+}CD45^{hi} macrophages/monocytes and CD11b^{+}CD45^{lo} microglia. Data are representative of three independent experiments. Each point represents an individual animal. P values were determined by One-way ANOVA with Tukey's post hoc test. Scale bars 200 µm for A-B, 20 µm for enlargements in A-B; 50 µm for C-F. dpi, days post immunization; F, females; M, males; prog, progression.

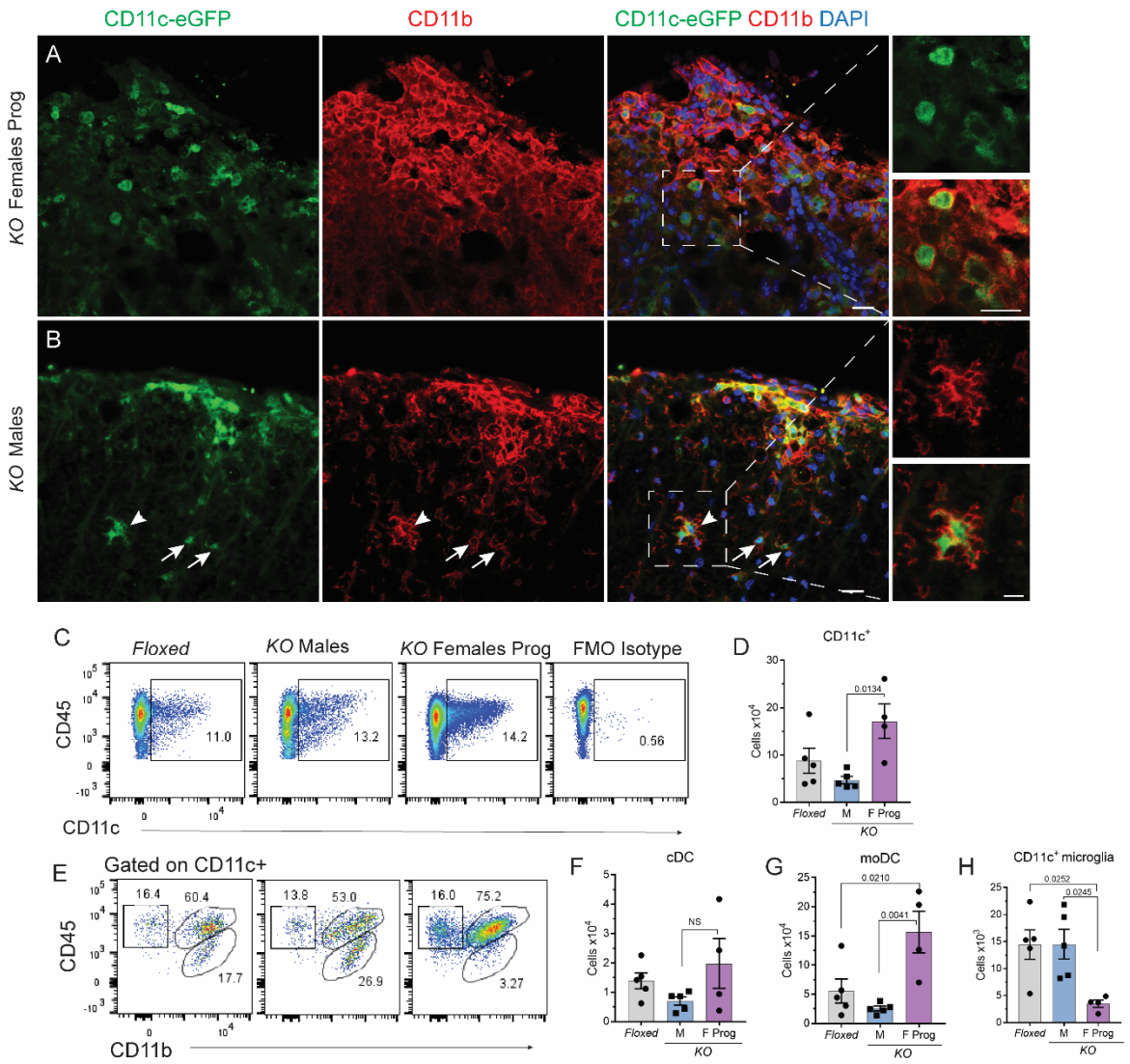

Fig. 6. Reduction in CD11c$^+$ microglia promotes EAE progression in *p38α* knockout females. CD11c$^+$ cells were visualized using CD11c promoter-driven expression of eGFP. (A) eGFP$^+$CD11b$^+$ cells with macrophage/reactive microglia morphology (enlargement) were localized in the lumbar spinal cord parenchyma of progressive *KO* females. (B) In *KO* males, eGFP$^+$ cells expressing CD11b were found detained at the meninges and partially reactive eGFP$^+$ microglia (arrows) were present in the parenchyma. Note distinct microglia with DC morphology (arrowhead and enlargement) in the white matter of the ventral lumbar spinal cord in *KO* males. (C) FACS analysis of CD11c$^+$ cells isolated from the brain and spinal cord of *floxed* mice, *KO* males and progressed *KO* females at 30 dpi. (D) Quantification of CD11c$^+$ cells. (E) FACS analysis of cDC, moDC and CD11c$^+$ microglia differentiated by CD45 and CD11b expression. (F-H) Quantification of cDC, moDC and CD11c$^+$ microglia. Data are representative of three independent experiments. Each point represents an individual animal. *P* values were determined by One-way ANOVA with Tukey's post hoc test. Scale bars 20 µm for A, B; 25 µm for enlargement in A; 10 µm for enlargement in B. dpi, days post immunization; F, females; M, males; prog, progression.

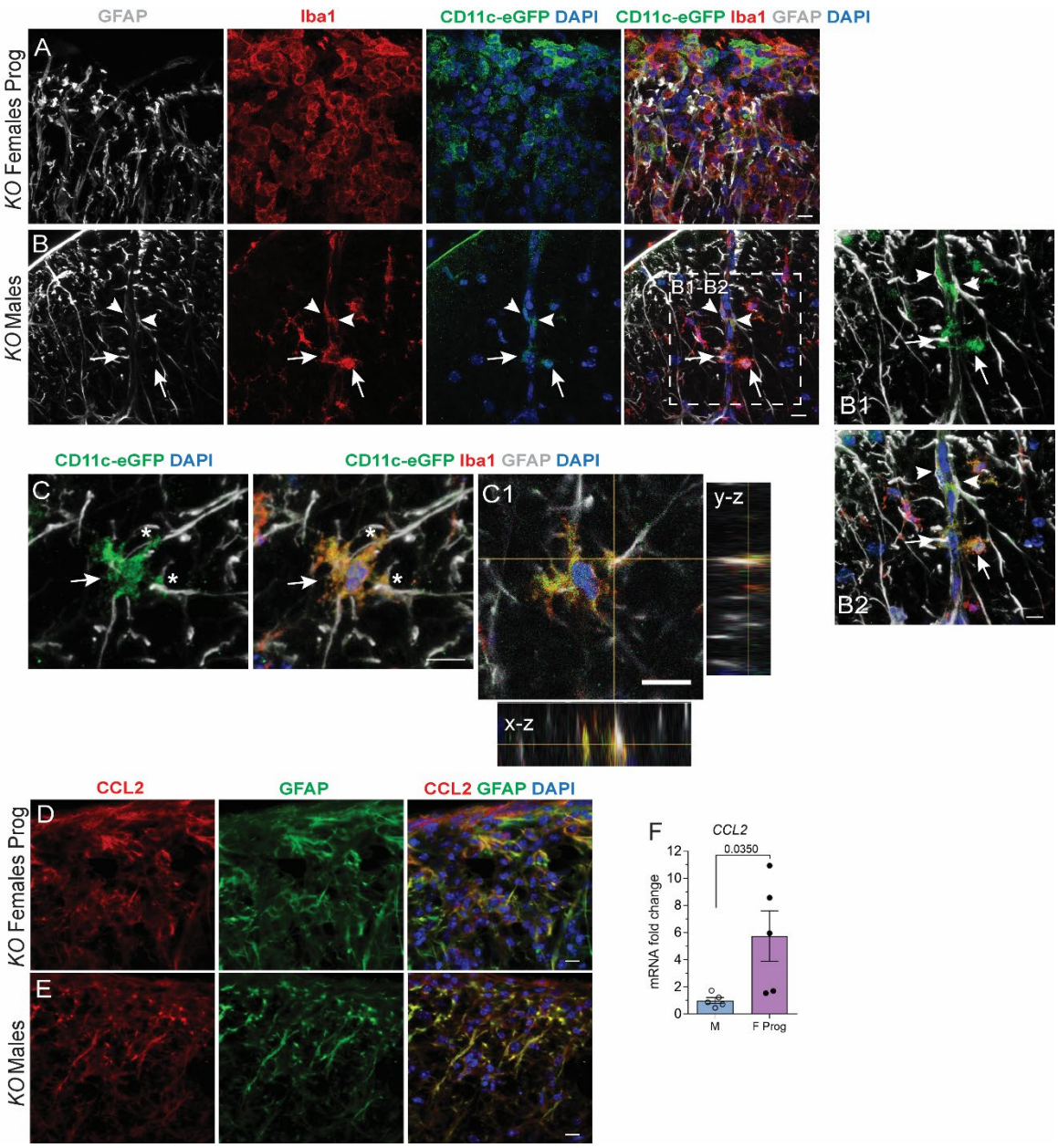

Fig. 7. CD11c$^+$ microglia are localized in close proximity to glia limitans.
CD11c$^+$ cells were visualized using CD11c promoter-driven expression of eGFP. (A) Hypertrophic processes of reactive astrocytes are surrounded by eGFP$^+$ moDC in the ventral spinal cord of progressed *KO* female mice. (B) In *KO* males, eGFP$^+$ microglia localize to perivascular areas outlined by glia limitans in the ventral spinal cord white matter of chronic mild EAE. (B1-B2, enlargements of B) Note distinct DC-like CD11c$^+$ microglia (arrows) in close proximity to glia limitans astrocytic endfeet and moDC (arrowheads) trapped within perivascular space. (C) In *KO* males, DC-like microglia (arrow) are located in direct contact (asterisks) to astrocytic processes in the spinal cord white matter of chronic mild EAE. (C1) Orthogonal projection showing close contact between CD11c$^+$ microglia and astrocyte processes. (D) CCL2 expression in hypertrophic reactive astrocytes in progressed *KO* females. (E) Reduced CCL2 expression in astrocytes in *KO* males. (F) mRNA transcription levels of CCL2 in the lumbar spinal cords of *KO* male and progressed *KO* female mice. Data are representative of three independent experiments. Each point represents one individual animal. Scale bars 10 µm for A-B, D-E; 20 µm for B1-B2, C-C1. P values were determined by Student's t-test. F, females; M, males; prog, progression.

Supplementary Figures

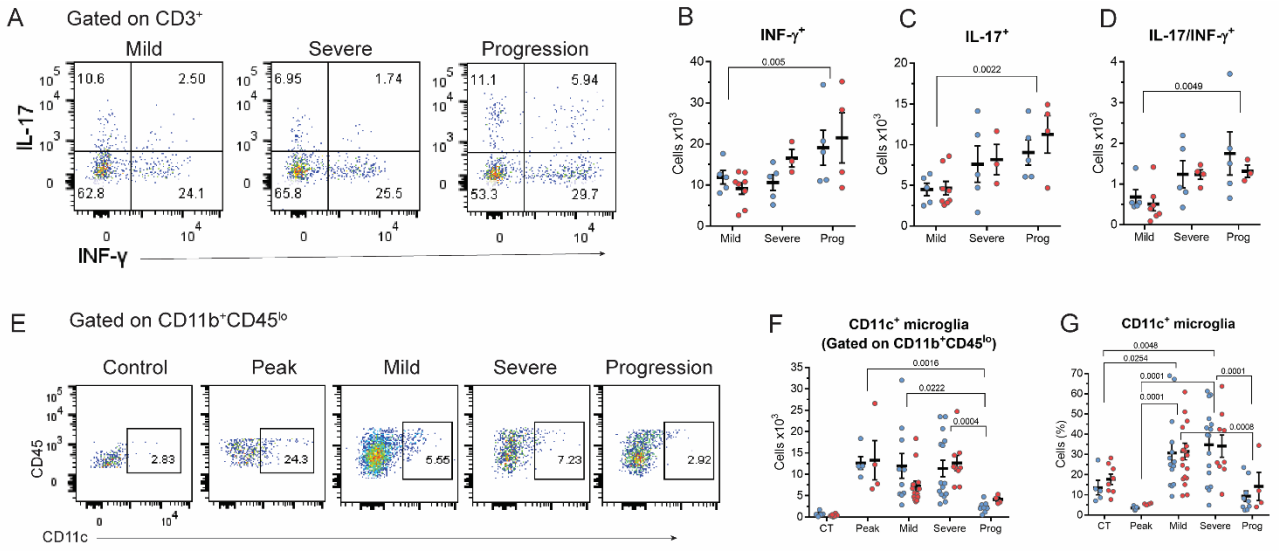

Supplementary Fig. 1. Increase in T cells and reduction in CD11c$^+$ microglia in EAE progression in WT mice.
(A) FACS analysis of T cell infiltrates in WT mice in mild, severe and progressive EAE at 30 dpi. (B-D) Quantification of IFN-γ$^+$, IL-17$^+$ and IL-17/IFN-γ$^+$ T cells. (E) FACS analysis of CD11c$^+$ microglia gated on CD11b$^+$CD45^{lo} microglia isolated from brain and spinal cord of healthy mice, at EAE peak, and chronic mild, severe and progressive EAE. (F) Quantification of CD11c$^+$ microglia gated on CD11b$^+$CD45^{lo} microglia. (G) Percentage of CD11c$^+$ microglia population among CD11c$^+$ cell population. Data are representative of three (for T cells) and six (for CD11c$^+$ microglia) independent experiments. Each point represents an individual animal. *P* values were determined by One-way ANOVA with Tukey's post hoc test. dpi, days post immunization; prog, progression.

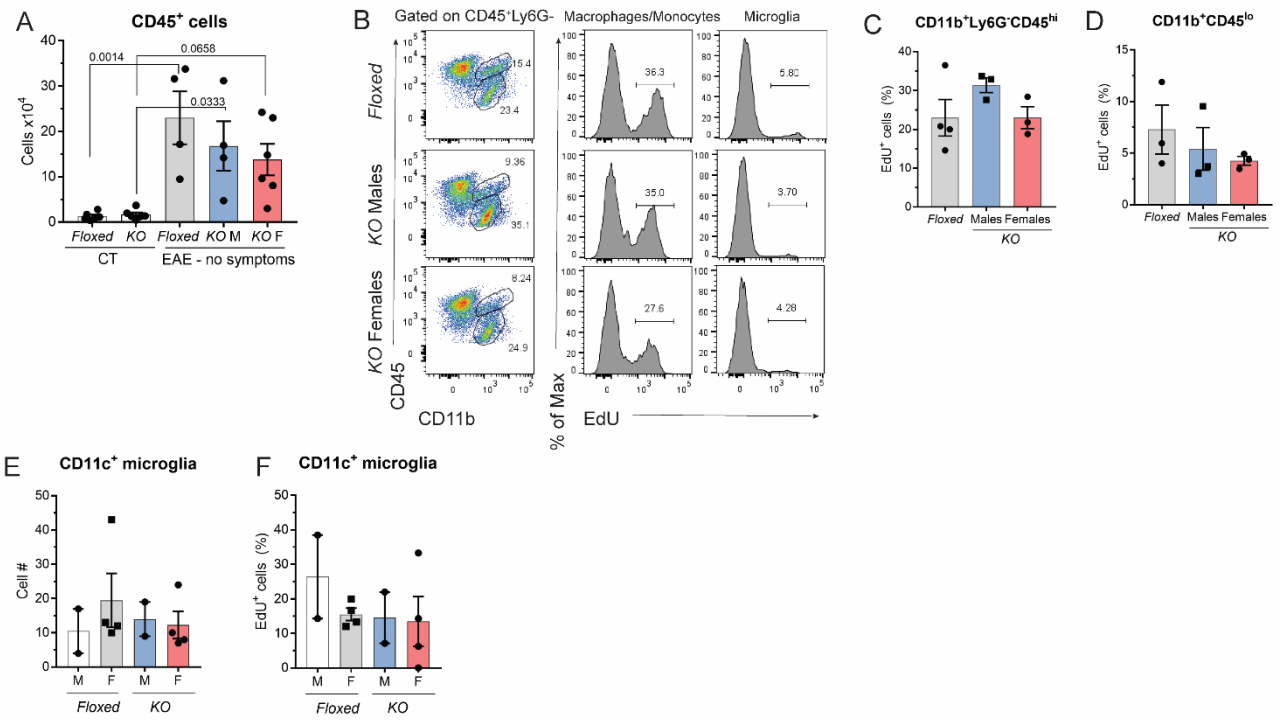

Supplementary Fig. 2. Proliferation of CNS immune cells during immune response.
Healthy mice and mice without EAE symptoms at 30 dpi were injected with 12 mg/kg EdU twice at 12 h interval. EdU$^+$ cells were analyzed 24 h after first injection. (A) Number of CD45$^+$ cells isolated from the CNS of healthy mice and mice without EAE symptoms at 30 dpi. (B) FACS analysis of EdU$^+$ macrophages/monocytes and microglia in the brain and spinal cord of MOG-immunized mice without EAE symptoms at 30 dpi. (C-D) Quantification of macrophage/monocyte and microglia proliferation rate of mice without EAE symptoms at 30 dpi. (E) Number of CD11c$^+$ microglia isolated from the healthy CNS of *floxed* and *KO* male and female mice. (F) CD11c$^+$ microglia proliferation rate in the healthy CNS of *floxed* and *KO* male and female mice. Data are representative of two independent experiments. Each point represents an individual animal. *P* values were determined by One-way ANOVA with Tukey's post hoc test. dpi, days post immunization; F, females; *KO*, knockout; M, males.

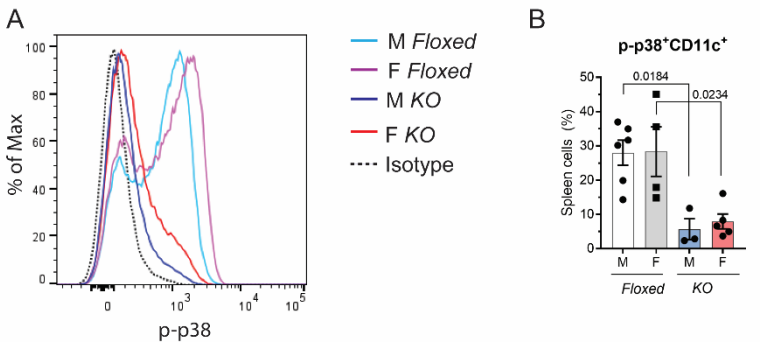

Supplementary Fig. 3. Reduction in p38 MAPK activity in *KO* mice.
Floxed and *KO* female and male mice were intraperitoneally injected with 3 mg/kg LPS 24 h before analysis. (A) Expression levels of the activated form of p38 MAPK, phospho-p38 MAPK (p-p38), was examined in $CD11c^+$ splenocytes by FACS. (B) Proportion of $p\text{-}p38^+$ $CD11c^+$ splenocytes of total spleen cells. Data are representative of two independent experiments. Each point represents an individual animal. *P* values were determined by One-way ANOVA with Tukey's post hoc test. F, females; *KO*, knockout; M, males.

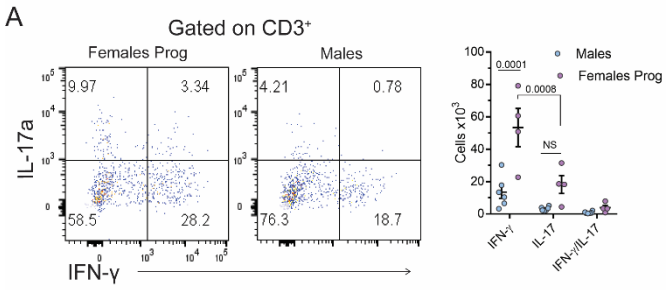

Supplementary Fig. 4. IFN-γ$^+$ cells comprise the majority of T cell population in progressed *KO* female mice.

(A) FACS analysis of IL-17a$^+$ and IFN-γ$^+$ T cells isolated from the CNS of *KO* male and progressed *KO* female mice. Data are representative of two independent experiments. *P* values were determined by Student's t-test. Each circle represents an individual mouse and small horizontal line indicates the mean. NS, not significant; Prog, progression.

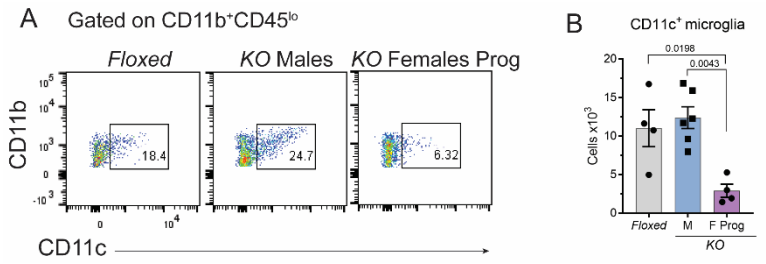

Supplementary Fig. 5. Reduction in CD11c$^+$ microglia population in *KO* female mice.
FACS analysis of CD11c$^+$ microglia isolated from the brain and spinal cord of *floxed* mice, *KO* males and progressed *KO* females at 30 dpi. (A) CD11c$^+$ microglia were gated on CD11b$^+$CD45^{lo} microglia. (B) Quantification of CD11c$^+$ microglia. Data are representative of three independent experiments. Each point represents an individual animal. P values were determined by One-way ANOVA with Tukey's post hoc test. dpi, days post immunization; F, females; *KO*, knockout; M, males; Prog, progression.